Analysis of the Effects of Changing Phase-lags and Montages on tACS E-fields

University of Twente, Davide S. Liuni (s2274515),
Committee: Dr. Ir. Bettina. C. Schwab, Dr. Ir. Jorien. T. W Berendsen and Msc. Ir. Silvana Huertas Penen

Transcranial alternating current stimulation (tACS) is a non-invasive brain stimulation technique that is currently being researched for its potential in treating various conditions. Controlling the electric field generated from tACS is critical for properly stimulating regions of interest in the brain. Simulations of dual site tACS were performed in SimNIBS for 16 subjects, to check the effects of changing phase-lags and electrode montages, on the field magnitude and distribution, when stimulating the primary motor cortices. The results showed no significant differences in magnitude when changing phase-lags while significant differences for the distribution. Three montages were then compared under different metrics to find the most suitable for stimulating the region of interest.

I. Introduction

Through decades of research, the electrical nature of the brain has been explored and partially mapped. From the local electrical mechanisms of single neurons and synapses, up to more global patterns. Neural oscillations are global signals from the brain that arise from synchronized firing of groups of neurons [1]. They can be detected with electroencephalography (EEG), by attaching electrodes to a person's scalp and measuring electric signals [2]. Advancements in research have made it possible to also modulate global oscillations, rather than just measuring them. This is relevant because neurodegenerative diseases and various prevalent conditions, including depression, anxiety, and substance use disorders, affect millions of people worldwide [3], and in these cases, neural oscillations differ from the norm [4].

A. Non-Invasive Brain Stimulation

Non-invasive brain stimulation (NIBS) methods utilize electrical or magnetic energy to non-invasively alter the activity of the brain's cortex [5]. They are thus categorized in transcranial electric stimulation (TES) or transcranial magnetic stimulation (TMS), depending on the chosen energy carrier, as shown in fig 1. Both have emerged as promising treatment techniques, since the induced fields can alter neural oscillations directly or indirectly. In TES, the brain is stimulated by placing electrodes on the scalp. Monitoring of brain activity is crucial when trying to analyze the effects of NIBS methods, EEG is thus often used for this purpose as a feedback mechanism [6].

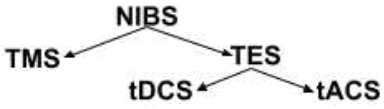

Fig. 1: Various Non-Invasive Brain Stimulation Methods

Electric current can either be direct (DC) or alternating (AC) depending on the source, this difference can thus differenciate between tDCS or tACS respectively. This paper focuses on tACS, however, due to the same underlying physics, tDCS is sometimes easier to take into consideration as a starting point, due to a more static effect.

B. tACS

In tACS, weak alternating electrical currents are applied to modulate neural oscillations, usually on the order of milli Amperes (mA). This is done through a current source that drives an alternating current through electrodes on the scalp [4]. A sine wave is a common signal applied to the electrodes tACS has shown potential in various applications, from enhancing cognitive functions to treating neuropsychiatric conditions [7]. A specific type of tACS, dual-site tACS (ds-tACS) injects weak alternating currents into two brain areas simultaneously, with the aim of modulating neural oscillations between the targeted areas, potentially influencing cognitive functions [7].

There are various parameters that can be adjusted when performing a ds-tACS, such as electrode montage and phaselags.

1) Montages: Electrode montages can differ in their size, shape, and the arrangement and number of electrodes. As will be discussed in the next section, the current at the electrodes creates an electric field. Placing the electrodes in different areas of the scalp, changes the electric field from tACS and activates different regions of the brain.

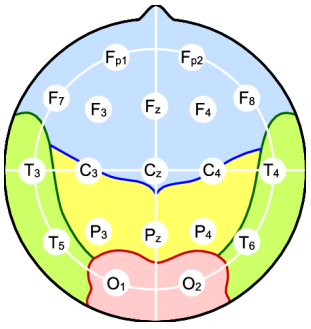

Fig. 2: EEG 10/20 System, taken from [8]

2) Phase Lag: A phase lag (ϕ) is a difference in timing between two signals, as shown in pic 3, the blue signal is ahead of the red one.

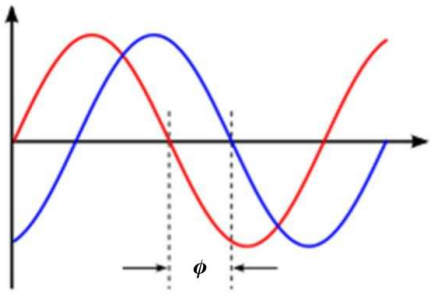

Fig. 3: Phase Lag, adapted from [9]

In the context of ds-tACS, the sinusoidal signals at the hemispheres can be made equal in time (in-phase), or shifted by various amounts (degrees or radians), with the most common configurations being a 0°shift (in-phase) and 180°shift (anti-phase) [1].

C. Motor Cortex

When applying tACS, intrinsic neural oscillations in the brain can be altered depending on the frequency, strength and positioning of the electrodes. The human cortex is the outer most part of the brain, comprised of 4 main lobes, and is the part of the brain that EEG measures the activity of [10], and that is stimulated by tACS. One area of the cortex is the primary motor cortex, abbreviated to M1, which sends signals to the muscles for movement. In a condition such as parkison's, some symptoms are due to abnormal neural oscillations at the motor cortex, among other areas. Applying tACS right above the primary motor cortex, could shine light on mechanisms to provide remedies for these conditions.

To understand how tACS affects the brain and how it can be optimized, a physical explanation of how tACS electrodes, and tES in general, interact with the brain will be analysed.

D. Electric Fields

In the context of brain stimulation, the most descriptive language to describe and analyze the electromagnetic force created by the electrodes is Electrodynamics and fields, rather than simply voltage and current, like in circuit theory. Fortunately, Electrodynamics has been complete theory for over a century [11, p. 15].

The principle of superposition, states that force felt by a test charge (Q), can be computed as the vector sum of the forces due to various charges q1, q2, q3, etc... [11, p. 59]

$$\mathbf{F} = \mathbf{F_1} + \mathbf{F_2} + \mathbf{F_3} + ... \tag{1}$$

The force given by a single charge, onto a second charge, was found through experiment and named Coulumb's law:

$$\mathbf{F} = \frac{1}{4\pi\epsilon_0}\frac{qQ}{r_1^2}\hat{r} \tag{2}$$

Where ϵ_0 is the permittivity of free space and r is the distance vector between the two charges. The electrical force between two charges is thus proportional to the product of charges and inversely proportional to the separation distance squared.

By combining these two, the concept of an electric field can be obtained:

$$\mathbf{F} = \mathbf{F_1} + \mathbf{F_2} + ... = \frac{Q}{4\pi\epsilon_0}(\frac{q_1}{r_1^2}\hat{r_1} + \frac{q_2}{r_1^2}\hat{r_2} + ...) \tag{3}$$

$$\mathbf{F} = Q\mathbf{E} \tag{4}$$

By changing the sum into an integral for a continuous charge distribution, the electric field of an electrode can be modelled as a volume charge, ρ.

$$\mathbf{E} = \frac{1}{4\pi\epsilon_0}\int \frac{\rho(r')}{r_1^2}\hat{r_1}d\tau' \tag{5}$$

A field, whether electric or magnetic, is "the force per unit charge that would be exerted on a test charge" [11], with units in [V/m = J/Cm = N/C] , depending on the test charge's position. Even for simple cases, this integral turns out to be extremely complex, hence the following section will lay out more ways for analysing the electric field created when applying current to tACS electrodes.

E. Maxwell's Equations

The way that electric and magnetic fields interact with charged objects and between one another are summarized by Maxwell's equations, written by Clark Maxwell in 1864, and later rewritten in more concise form with the Nabla operator (∇). These are the equations for fields in a vacuum.

$$\nabla \cdot \mathbf{E} = \frac{\rho}{\epsilon_0} \tag{6}$$

$$\nabla \cdot \mathbf{B} = 0 \tag{7}$$

$$\nabla \times \mathbf{E} = -\frac{\partial \mathbf{B}}{\partial t} \tag{8}$$

$$\nabla \times \mathbf{B} = \mu_0(\mathbf{J} - \epsilon_0\frac{\partial \mathbf{E}}{\partial t}) \tag{9}$$

The first two equations describe the divergence of the electric and magnetic fields. Divergence is a measure of a field's outward dispersion or inward collection [11]. In the left side of fig 4, the positive charge in red displays a positive divergence, with the arrows radiating outwards, while the opposite happens with the negative charge, with the arrows pointing inwards. This is explained in eq 6, Gauss' law, where the charge density ρ, and it's polarity determine the divergence of the field. Gauss's law (6) is derived by combining Coloumb's law (2) and superposition (1). The second equation explains why there can be no magnetic monopoles, and why there must always be a north and south pole, as shown in the right of figure 4. Since the field lines always close in a loop, there will never be a positive or negative divergence, as the net effect will always be zero. In contrast, the positive electric charge on the left of fig 4 could exist by itself, thus having a positive divergence.

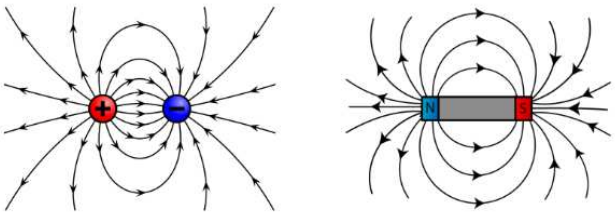

Fig. 4: Electric and Magnetic Divergence, taken from [12]

F. Quasi-Static Assumption

In dual-site tACS and TES in general, the quasi-static assumption can be applied, which neglects the coupling between electric and magnetic fields, and thus neglecting the effect of electromagnetic waves, when the stimulation frequency is below 5kHz. This simplification effectively removes equations 8 and 9, since they deal with how changing E-Field or B-Field affect each other, leading to EM waves. This approximation is rooted in the fact that the wavelength of the EM field is significantly larger compared to the size of the region of interest in tACS, the motor primary motor cortex in this case [13]. The wavelength of an EM wave is given by the constant speed of light (c), over the frequency of propagation. With a stimulation frequency of 5kHz, that would provide a wavelength of 60km, compared with a region of interest of a few centimeters.

$$\lambda = \frac{c}{f} \tag{10}$$

$$\frac{3 \cdot 10^8}{5000} = 60km \tag{11}$$

As a result, any phase variation of the EM field across this region is negligible.

With this simplification in mind, the analysis and calculation of the E-fields become considerably easier. Essentially changing the relevant Maxwell's equation to:

$$\nabla \cdot \mathbf{E} = \frac{\rho}{\epsilon_0} \tag{12}$$

$$\nabla \times \mathbf{E} = 0 \tag{13}$$

A study conducted by IEEE [13], analyzed the accuracy of this framework by comparing the answers it provides with the full set of Maxwell's equations listed before, and concluded that there is a difference below 1%, while considerably reducing the computational load in simulations. The study also analyzed a second assumption that is ubiquitous in this field, namely modelling the brain as purely ohmic and ignoring any capacitative effect, and found this second assumption to be more problematic.

G. Electric Potential

Gauss's law is effective for calculations when geometrical symmetry can be utilized, such as an infinitely long plate or a sphere [11] For more real life scenarios, such as a charge distribution from electrodes of a finite volume, it's easier to instead work with the electric potential, which is a scalar quantity, and then calculate the electric field from it, as is done in the FEM simulations in section III

The curl of E is zero in the static and quasi-static case (eq (13), which means that it is a conservative field [10]. Due to Stokes theorem, the line integral around any closed loop in a conservative field is equal to zero [11], meaning that no field lines can close in themselves [10]. This makes it possible to define a scalar field from the vector field $\mathbf{E}$, which is the electric potential:

$$\mathbf{E} = -\nabla \cdot V \tag{14}$$

The scalar electric potential V assigns a number to every point in space, a difference in potential between two points is a voltage difference, measured in Volts [10].

When a charge is present, Gauss's law can be combined with eq (14) to reach Poisson's equation (16)

$$\nabla \cdot \mathbf{E} = \nabla \cdot (-\nabla V) = -(\nabla^2 V) \tag{15}$$

$$\nabla^2 V = -\frac{\rho}{\epsilon_0} \tag{16}$$

In cases where there is no charge, or is assumed to have no charge, Poisson's equation simplifies to Laplace's equation (17)

$$\nabla^2 V = 0 \tag{17}$$

These equations, after being altered by including the effect of a conductive medium, such as a human head, are crucial for calculating how the electric fields from tACS changes when interacting with a scalp.

H. tACS E-Field Analysis

When applying tACS, the alternating electric currents from the electrodes create a changing electric field, since the volume charge at the electrodes oscillates in time depending on the signal from the current source. Because of the quasi-static assumption, the coupling of the E and B fields can be neglected, and the effect of the changing B-field onto the E-field can be approximated to zero through 13. It is thus possible to consider the changing electric field at one electrode as a sequence of electrostatic 'snapshots' or static E-fields in time, represented by Gauss's law changing in time:

$$\nabla \cdot \mathbf{E}(t) = \frac{\rho(t)}{\epsilon_0} \tag{18}$$

When the tACS signal is at the peak of the sine wave, the generated E-field at that point in time will be at the maximum, and when it's zero the E-field will be zero at that instance.

When considering electrode montages, multiple electrodes are placed on a scalp, and in dual-site tACS, multiple electrodes are placed on each hemisphere. Due to superposition, the combined E-field created by the electrode montage can be calculated as a linear combination of the field of each electrode.

When introducing phase-lag between the hemispheres, the electric fields from each side interfere with each other in

constructive and destructive manners, depending on each side's direction and strength at a given instance and point in space.

The combined electric field from the electrodes, if placed in a vacuum, would simply decay as a function of distance due to the inverse square law present in Columb's law. Considering a static tACS instance, when placing a human head inside the field, the field at this instant is not only a function of distance, but also of how the field interacts with the charges in the head.

The electric potential, Poisson and Laplace's equation (14, 16, 17), are used in the calculation of the E-field in the simulation. However, due to the human head being a conductive medium, with varying conductivities the equations have to be adjusted to include the propagation of current inside the head. This current can be described by the continuous version of Ohm's law (19), and plugging it in the divergence of $\mathbf{J}$ to get (20).

$$\mathbf{J} = \sigma \mathbf{E} \tag{19}$$

$$\nabla \cdot \mathbf{J} = \nabla \cdot (\sigma \mathbf{E}) = -\nabla \cdot (\sigma \nabla V) = 0 \tag{20}$$

Due to the complexity of these calculations, further analysis of the Electric Field will be done in the Methoddoloogy, using the derived equations in a discredited way, to compute tACS simulations through software.

I. Electrical Model of a Neuron

The mechanisms by which the E-fields in tACS, and TES in general, affect the brain, are highly intricate and still a topic of debate. The brain is incredibly complex and analysing the precise mechanisms of how tACS affects the brain is outside the scope of this paper. However, to provide a glimpse of these mechanisms, a simplification of the electrical transmission in the brain and the current stance found in literature of the effects of tACS will be shortly layed out and summarized. This will help underscore the importance of carefully analyzing E-fields from tACS in the research question, and also point to the important features of the E-field to analyze. To keep it concise, only the electrical nature of neuron transmission will be discussed, leaving out any chemical aspects, such as neurotransmitters, and also leaving out other cell types or even different neuron types.

A human brain is made up of approximately 86 billion neurons, the standard cells of the nervous system [14], depicted in fig 5.

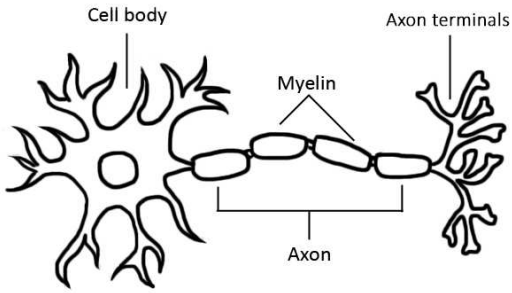

Fig. 5: Simple Depiction of a Neuron, taken from [15]

Through an electrical engineering lense, the neuron can be viewed as a system with various inputs, called dendrites, next to the cell body, and conductive cable, called the axon and output terminals called the axon terminals. The connection between a neuron's axon terminals (output) and the next neuron's dendrites (input) is called a synapse. In this simplistic electrical model, a neuron's function is to propagate a signal, from the dendrite to the axon terminals, to then propagate it to the next synapse. This simpler model can be depicted as in fig 6. In reality, neurons have thousands of dendritic fibrils and similarly many axon terminals [14].

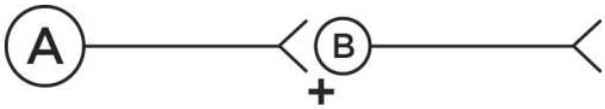

Fig. 6: Electrical Model of a Neuron, taken from [14]

The resting electrical state of a neuron, called the resting potential, is interestingly not zero, but -70mV. It is the potential difference between the inside of the neuron and the outside [14]. In order for a neuron to go from a resting potential, to an excited propagation state, called an action potential, enough of the dentrites need to be depolirized at the synapse. When enough inputs depolarize the start of the axon, the axon hillhock, from -70mV to -40mV, a change in state happens in the neuron, where different pumps move ions out and polarize the axon to 30mV, and propagating this signal to the axon terminals [14].

In this simplified model, the neuron acts a sort of integrator, taking in lots of inputs, summing them and propagating a single output to various axon terminals once a threshold is reached. The input stage, from dendrites to axon hillhock can be viewed as an analogue signal, while the propagation of the action potential can be viewed as a digital signal (of 30mV) switching on once the input polarization reaches -40mV.

This was the simplified electrical mechanism of a single neuron, hundred or thousands of neurons create local groups called ensembles, zooming out again and the brain can be split in anatomically or functionally differentiated regions [1]. When EEG is applied, it does not measure the activity of a single action potential or synapse, but rather the more global

electrical activity of the brain. Neural oscillations are periodic, wave-like variations in the brain's electrical activity [4]. These oscillations are a manifestation of the synchronized activity of neuronal ensembles, firing in a coordinated manner.

J. tACS E-fields affecting the Brain

In the simpler case of tDCS, the direct current at the electrodes creates a static field, which can be visualised with the simple electrical model of the neuron in Figure 24.

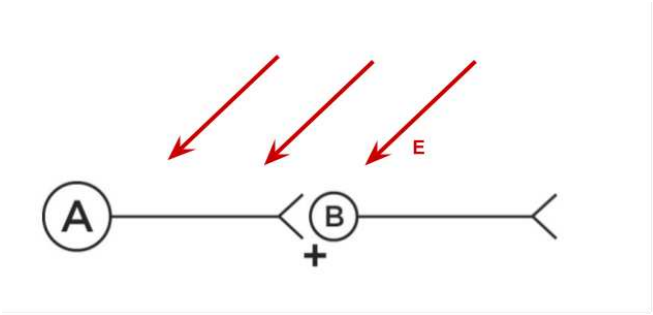

Fig. 7: Electrical Model of a Neuron with an E-field from tDCS, adapted from [14]

This field is thought to alter the electric charge difference across a neuron's membrane, the resting membrane potential [16]. It creates a force on the neuron's ions that make up the resting potential, which can calculated by Coulumb's law from eq (2). It thus leads to a movement of the ions. Depending on the direction and strength of the field, and the cumulative effect that it has on the ions, it could either polarize or depolarize the neuron from -70mV. The neuron could then require less or more input exitation than before to reach the–40mV threshold at the axon hillhock. If the field it's parallel to the neuron, it could move ions towards the axon hillhock, while if it's perpendicular, it could cause more localized effects, so the direction of the field can influence the amount of polarization.

This is relevant because the human cortex, as depicted in figure 8, contains long pyramidal neurons [10], and the orthogonality of the field with respect the to the neurons will thus modulate the effects of tACS. This is why in the Methodology, the normal component of the E-field with respect to the cortex is calculated.

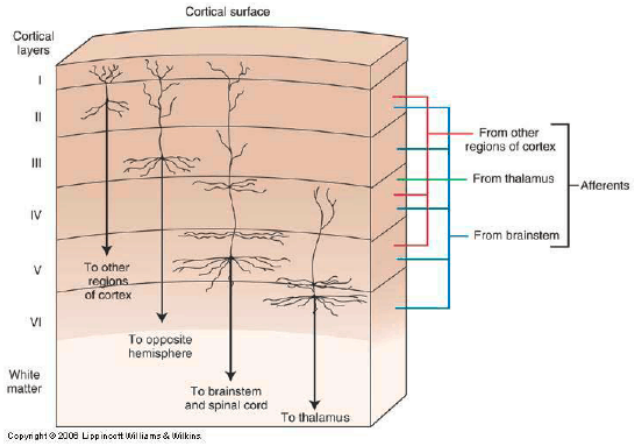

Fig. 8: Pyramidial Neurons in the Cortex, taken from [15]

The exact effect of the E-field and potential polarization of a single neuron depends the resulting movement of ions and the strength and direction of the E-field at that point in space. At the more global level, there are a lot of other effects that an induced electric field from the electrodes causes, such as stimulating multiple areas simultaneously, which has made it hard to replicate results from studies and find a complete explanation for the seen effects of tDCS [17].

For tACS, since the E-field changes in time, $\mathbf{E}(t)$, the picture is even more complex, and the effect on the resting potential is, therefore, more transient and also changing in time. One hyphotesis for tACS is that it is thought to modulate neural oscillations by neuronal entrainment. In this context, entrainment is a one way synchronization between external stimuli, ie a changing electric field, and a system, such as the brain or a group of neurons[18]. A notorius example of entrainment is circadian rhythm, ubiquotus throughout nature.

Study [17] notes how inferring causality between E-field created in tACS, or TES in general, creates a complex and convoluted chain of causalities, which make it hard to pinpoint the exact mechanisms of tACS and what exactly causes the behavioral effects seen in many studies. The mechanisms of how tACS affect the brain will, thus, not be explored further, but the focus will be restricted on the generated E-field, and some more specific metrics will be layed out in sections III, to further analyze the E-field. The effect of different tACS configurations, such as changing the phase of ds-tACS or electrode montage, will be analyzed through the change in the E-field metrics.

II. Problem Statement and Research Question

When tACS is applied, control over the E-field, such as its magnitude or its distribution in the scalp are critical for targeted approaches, especially due to discussed complexity of the resulting effects of the generated E-field.

The main goal of this paper is to find out how phase-lags and electrode montages affect the distribution and amplitude of the E-field generated when stimulating the primary motor cortices with ds-tACS. Considering the broad scope of this

main research question, it will be approached by answering sub-questions for each independent variable (phase-lag and electrode montage).

Phase-Lag Parameter Analysis

For Phase-Lags ($\phi = 0$, $\phi = \pi/4 = 0.79$, $\phi = \pi/2 = 1.57$, $\phi = 3\pi/4 = 2.36$, $\phi = \pi = 3.14$, $\phi = 5\pi/4 = 3.93$, $\phi = 3\pi/2 = 4.71$, and $\phi = 7\pi/4 = 5.50$):

- How do different phase-lag values affect the average electric field strength and distribution in the cortex and primary motor cortices?
- Is the effect of phase-lag variations on the electric field strength and distribution statistically significant?

Montage Configuration Analysis:

- What is the influence of different montage configurations on the average electric field strength in the primary motor cortex? Is there a montage that is best suited for stimulating the primary motor cortices?
- How does each montage configuration affect the distribution of the electric field in the primary motor cortex and the cortex overall?
- Which electrode montage configuration yields the most uniform electric field strength across the bilateral primary motor cortices, accounting for hemispheric anatomical variations?

The three montages to be analyzed are shown below, following the 10/10 electrode positioning system. They are symmetrycal between the hemispheres, with a central electrode and 3 electrodes surrounding it on each side, an example is given in the appendix, figure 27.

Montage 1	Montage 2	Montage 3
C4, FC4, C2, CP4	CP4, C4, P4, CP2	CCP4h, FCC4h, CP2h CPP4h
C3, FC3, C1, CP3	CP3, C3, P3, CP1	CCP3h, FCC3h, CP1h CPP3h

Fig. 9: Simulated Electrode Montages

III. Methodology

In order explore these questions, simulation of tACS will be performed in SimNIBS. The simulations codes were created and provided by Silvana Huertas Penen, with the calculation of the E-field metrics described later in III-A as well.

SimNIBS is a program that creates individualized simulation models by taking MRI scans of people's scalps, and turning them into a Finite Element Model (FEM) [19]. This study's dataset includes MRI scans from 16 individuals, featuring both T1 and T2 types, conducted at 3T field strength. These scans are part of the 1200 Human Connectome Project (HCP) [20].

A model of the brain is composed of hundred of thousands of tetrahedrons, as shown in figure 11. It is then segmented into six different categories of tissue, with different conductivies, namely: Scalp, Compact Bone, Spongy bone, Cerebrospinal fluid, Gray matter, White matter. Figure 10 shows the different types of conductive tissues used in the models and their corresponding conductivity value in [S/m].

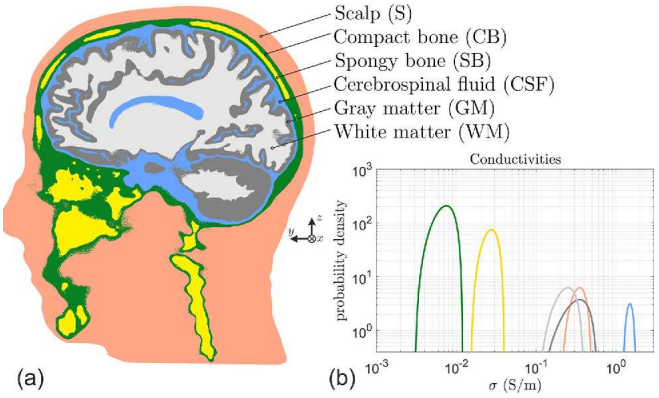

Fig. 10: Segmentation, taken from [21]

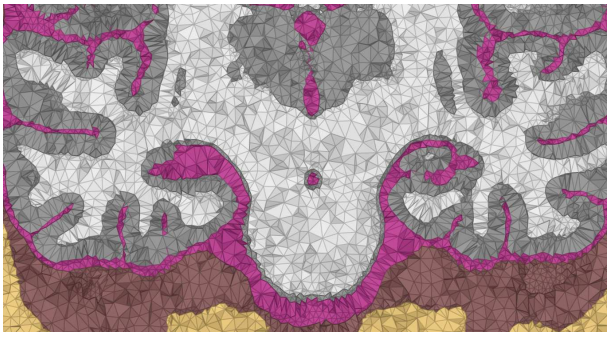

Fig. 11: Tetrahedrons, taken from [22]

The equations from Section I-E are continuous, SimNIBS numerically solves these equation at each tetrahedron or node of the tetrahedrons. The head is thus modelled as a combination of thousands of these tetrahedrons of different conductivities, but assuming no conductive effects, which could be present in real life. Because of the quasi static assumption and solely ohmic conductor model, the temporal and spatial components of the E-field can be separated [19]. The principle of superposition from (1) can be used to further separate the contribution for N electrodes.

$$\mathbf{E}(\mathbf{p}, t) = \mathbf{E}(\mathbf{p})I(t) \tag{21}$$

$$\mathbf{E}(\mathbf{p}, t) = \sum_{i=1}^{N} \mathbf{E}(\mathbf{p}, t) = \sum_{i=1}^{N} \mathbf{E_i}(\mathbf{p})I(t) \tag{22}$$

These principles are used to derive the equation used in the simulations (23). To reduce the computational load of the simulations, they are split in three separate partial simulations, as shown in figure 12, and then combined together through (23). This division is based on paper [23]

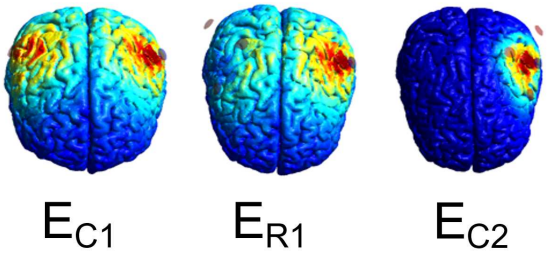

Fig. 12: Separate simulations, made by Silvana Huertas Penen

For a given montage, the first partial simulation (C1) calculates the field while considering only the central electrodes. The second partial simulation (R1) is then subtracted from the first, thus eliminating the contribution from central electrode of the left side of C1. This makes it possible to add the complete left side of the montage as a last step in C2, and adding the phase-shift of ϕ there, as adding it on both sides would make the two sides always in-phase.

$$E(p,t) = I_0(E_{C1}(p)sin(2\pi ft) - E_{R1}(p)sin(2\pi ft) + E_{C2}(p)sin(2\pi ft + \phi)) \quad (23)$$

A. E-Field Metrics

To answer the questions layed out in the problem statement, two metrics are calculated and measured.

1) Magnitude: The first metric, is the magnitude of the electric field, which can be calculated by Pythagoras theorem in three dimensions.

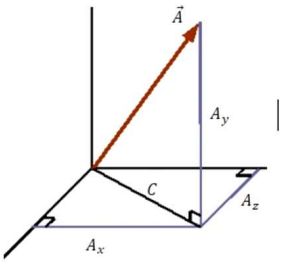

$$||\mathbf{A}|| = \sqrt{A_x^2 + A_y^2 + A_z^2}$$

Fig. 13: Magnitude of a 3d vector, taken from [24]

This is useful to analyze which regions of the brain that are most affected by the stimulation, and to make sure that the wanted regions of interest are targeted.

2) Relative Distance Measured (RDM): This second metric quantifies the similarity between two spatial electric field distributions. This measure is also taken from [23]

$$RDM = \left\| \frac{|\mathbf{E_n^{in}}|}{\|\mathbf{E_n^{in}}\|} - \frac{|\mathbf{E_n^{\phi}}|}{\|\mathbf{E_n^{\phi}}\|} \right\| = \sqrt{\sum \left(\frac{|\mathbf{E_n^{in}}|}{\|\mathbf{E_n^{in}}\|} - \frac{|\mathbf{E_n^{i}}|}{\|\mathbf{E_n^{i}}\|} \right)^2}$$

The RDM goes a step further because it compares the magnitudes of an electric field at each point, taking the difference of every single vector in the electric field for a baseline condition, in-phase in this case, and comparing it to various phase-lags. This difference is normalized by the vetor's norms in the denominator, then all the squared differences are summed, to provide a positive result. An RDM of 0 means that two electrical field distributions are identical, since all the differences were equal to zero, while an RDM of $\sqrt{2}$ is the maximum value, meaning very dissimilar distributions [23]. In the results, all RDM values are calculated for the normal component of the Electric field with respect to the cortex, due to the direction of the pyramidal neurons depicted in 8. An assumption for tACS is that varying phase, should have limited effects on the field [1]. This should be true for both magnitude and RDM. Due to this, the lowest RDM possible for a given montage would be preferred.

B. Statistics

1) Statistical Tests for Different Phase-Lags ϕ: The first step in analyzing the effect of varying phase-lags on the electric field metrics was done through statistical testing, to check weather the change in the metrics from the different phase-lags was statistically significant, using ANOVA and non-parametric equivalent tests. These test check whether the variance between a single phase-lag (within group) can explain the variation between different phase-lags (between groups). If not, then the results are statistically significant because the changing the independent variable, in this case the phase-lag, changed the results more than the variation of a single phase-lag. A full flowchart of the steps taken is shown in the appendix, figure 28.

2) Montage Measures:

- The first relevant value to be calculated is the average magnitude at the left and right motor cortices ($\frac{L+R}{2}$). An example result for the simulations of a single subject is shown in figure 23 in the appendix, showing the average over time of the maximum magnitude for each phase-lag. The values from those plots are averaged for the 16 subjects and for all phase-lags. So an Average, of the average in time of the maximum magnitude, across the primary motor cortices, is a more complete description.
- When interested in the stimulation of the primary motor cortices, it is relevant to know if the maximum field is happening in these regions, thus a comparison between the maximum field strength at the whole cortex and primary motor will be made.
- A difference in the strength of the field between the two primary motor cortices on each hemisphere was noticed while running the simulations. A montage with the lowest difference between the two, could be seen as more robust to anatomical variation between the hemispheres, thus an asymmetry index is calculated

$$Asymmetry\,[\%] = \frac{|L-R|}{(L+R)/2} * 100 \quad (24)$$

- The last data point to analyze is the montage with the lowest RDM for all phase-lags, as this is better for tACS.

The results will be presented sequentially, in the same order as just described.

IV. Results

A. Effect of changing Phase-Lag

The first result to note is that all measured results are symmetrical around π radians. The statistical test result for different phase-lags, turned out to be from the non-parametric part of the flow chart in figure 28, since most of the data did not follow a normal distribution. For the magnitude, the statistical results showed no statistical significance when changing the phase-lag, this could be explained by the fact that, as shown in figure 14, the standard deviation within a phaselag is quite large compared to the change in mean between phaselags. Becuase of this large difference within a phase-lag, it becomes hard to detect changes between phase-lags, at least for this sample size. The same is not true for the RDM, as the standard deviation is quite small compared to the change in mean value, and statistically significant results for all phase-lags except 0.79 and 5.50 [rad] are shown in figure 30 in the appendix.

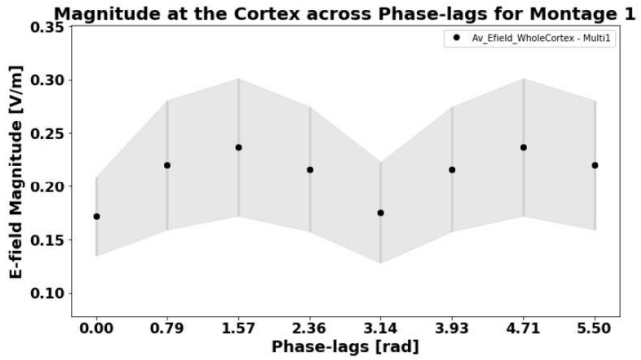

Fig. 14: Average Field Strength Mean and Standard Deviation for Montage 1

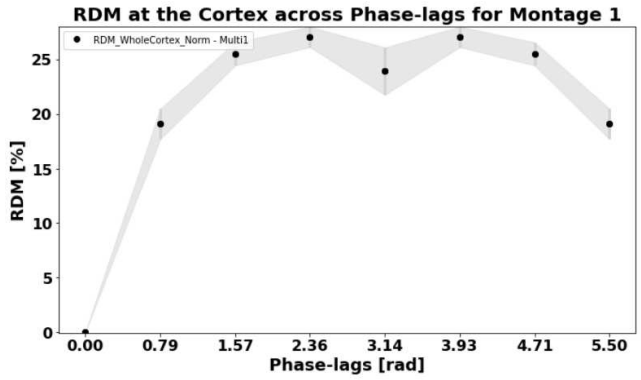

Fig. 15: RDM Mean and Standard Deviation for Montage 1

Thus changing phase-lag does change the RDM, in a statistically significan way, even by almost 30% in some cases, when comparing it to the in-phase condition.

B. Montage Comparison

- The montage with the greatest average over time of the maximum field strength at the motor cortices was Montage 1. The box plot shows the average magnitude at the primary motor cortices, as the height of the box, and the standard deviation between the 16 subjects shown by the vertical whiskers.
- Figures 17, 18 and 19 display the difference between average magnitude in the Cortex (green) and primary left and right motor cortices (blue and orange) for each phase lag. The dots are the means for the 16 subjects, with the vertical line being the standard deviation. The closer the average field strength of the primary cortices is to the average strength of the whole cortex, the more a montage ”focuses” the field onto the primary motor cortices, rather than stimulating other areas more, such as in montage 2, figure 18. Again, Montage 1 is better suited for stimulating the primary motor cortices with respect to montage 2, and because of the box plot in figure 16, also compared to montage 3.

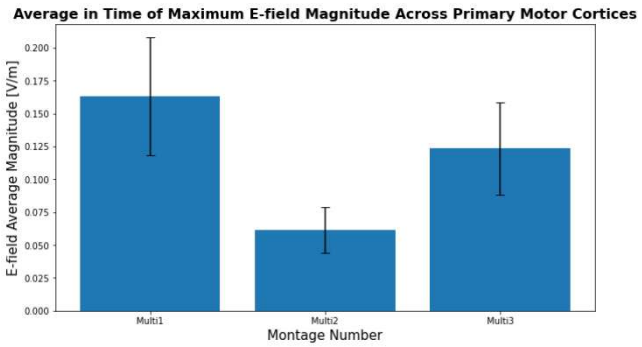

Fig. 16: Box Plot comparing Montages for Average Magnitude in the Primary Motor Cortices

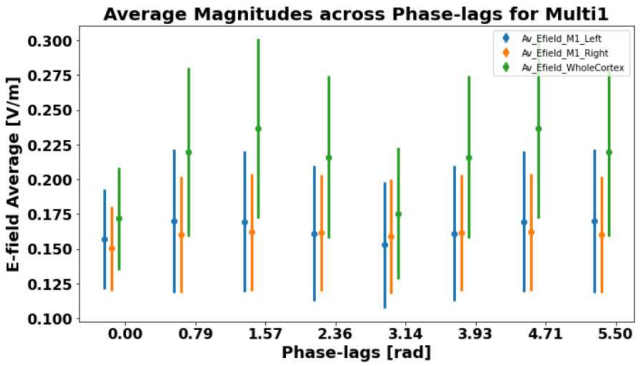

Fig. 17: Cortex vs Primary Motor Cortex av Field Strength Montage 1

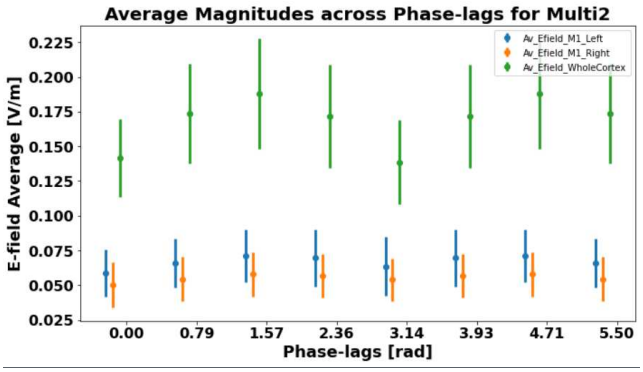

Fig. 18: Cortex vs Primary Motor Cortex av Field Strength Montage 2

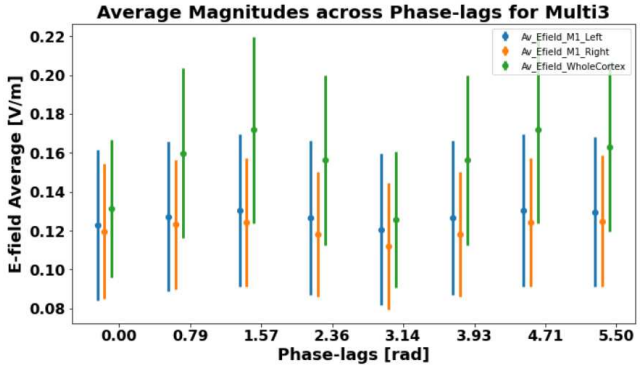

Fig. 19: Cortex vs Primary Motor Cortex av Field Strength Montage 3

- Regarding the Asymmetry between the left and right primary motor cortices, a difference was noted, as shown in figure 20, which shows again montage 2 as more problematic, while a similar results for montages 1 and 3.

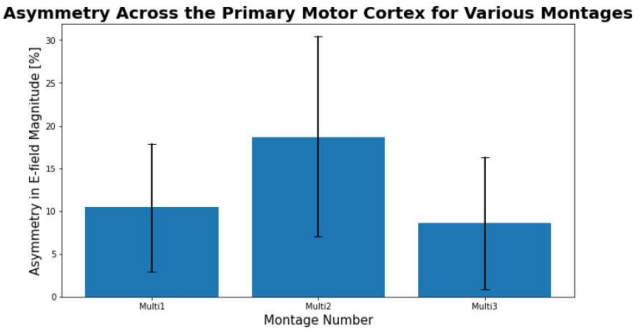

Fig. 20: Asymmetry Index

- Figure 21 shows the RDM values averaged for all subjects and all phase-lags. As explained in the methodology, due to tACS assumptions, a montage with the lowest RDM for all phase-lags would be preferred. The RDM for the whole cortex is similar for all montages, however it is lowest in montage 1 for the primary motor cortices.

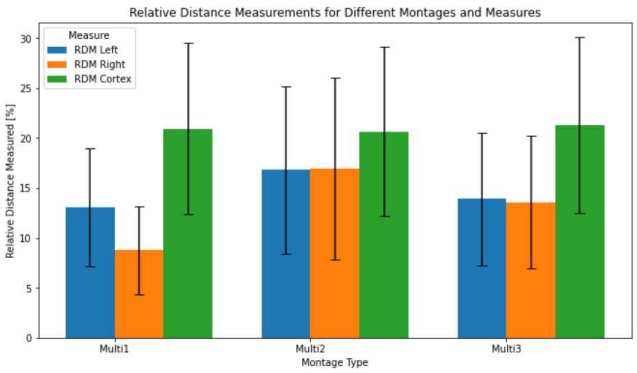

Fig. 21: Results for Magnitude

V. Conclusion

To conclude, changing the phase-lag in ds-tACS did not change the average field strength at the cortex or primary motor cortices in a statistically significant way, due to the high standard deviation between the subjects. For the RDM the statistical result tests showed significance for all phase-lags except 0.7854 [rad], as shown in figure 30. This means that altering the phase-lag does have an effect on the distribution.

The montage results indicate that Montage 1 and Montage 3 achieved similar results while Montage 2 was inferior under all comparisons: overall magnitude in the primary motor cortices and in relation with the whole cortex, asymmetry and RDM. Montage 1 produced the greatest average electric field strength at the primary motor cortices, visualized in a box plot (Figure 16), and had a lower RDM than Montage 3 for the right primary motor cortex. Due to these results, montage 1 would be better suited for stimulating the primary motor cortices than montage 2 and 3.

VI. Discussion

In this study, some insights into how various phase-lags and montages affect a simulated electric field magnitude and distribution around the cortex and the primary motor cortices in tACS were gathered.

Initially, an orthogonality measure was supposed to be included, as mentioned in the appendix, which would have provided another way to analyze the tACS simulations. Additionally, an effect known as a traveling wave, a changing E-field magnitude peak location, was being investigated for certain phase-lags such as $\pi/4$. Both of these were scrapped due to time restraints and the long run times of the 48 simulations made. They would have added more depth to the analysis and could definitely be included in future research. Another critically important point that was not discussed in this research is the importance of individual anatomy on tACS and NIBS in general. Statistics could have been performed by finding correlation measures between the amount of gray matter of a subject, taken as the number of tetrahedrons in that conductivity type, and various metrics. Including the meshes themselves in the analysis could have vastly increased the level of insight.

REFERENCES

[1] I. Alekseichuk, A. Y. Falchier, G. Linn, T. Xu, M. P. Milham, C. E. Schroeder, and A. Opitz, "Electric field dynamics in the brain during multi-electrode transcranial electric stimulation," *Nature Communications*, vol. 10, no. 1, 2019.

[2] A. Biasiucci, B. Franceschiello, and M. M. Murray, "Electroencephalography," *Current Biology*, vol. 29, no. 3, Feb 2019.

[3] Dec 2020. [Online]. Available: https://www.who.int/news-room/fact-sheets/detail/the-top-10-causes-of-death

[4] O. Elyamany, G. Leicht, C. S. Herrmann, and C. Mulert, "Transcranial alternating current stimulation (tacs): From basic mechanisms towards first applications in psychiatry," *European Archives of Psychiatry and Clinical Neuroscience*, vol. 271, no. 1, p. 135–156, 2020.

[5] E. Dayan, N. Censor, E. R. Buch, M. Sandrini, and L. G. Cohen, "Noninvasive brain stimulation: From physiology to network dynamics and back," *Nature Neuroscience*, vol. 16, no. 7, p. 838–844, 2013.

[6] A. V. Tavakoli and K. Yun, "Transcranial alternating current stimulation (tacs) mechanisms and protocols," *Frontiers in Cellular Neuroscience*, vol. 11, 2017.

[7] G. Soleimani, R. Kupliki, J. Bodurka, M. P. Paulus, and H. Ekhtiari, "How structural and functional mri can inform dual-site tacs parameters: A case study in a clinical population and its pragmatic implications," *Brain Stimulation*, vol. 15, no. 2, p. 337–351, 2022.

[8] D. P.-O. Bos, "Figure 3: 10-20 system of electrode placement. - researchgate," Jan 2006. [Online]. Available: https://www.researchgate.net/figure/10-20-system-of-electrode-placement_fig3_237777779

[9] Peppergrower, "File:phase shift.svg," 2009. [Online]. Available: https://en.m.wikipedia.org/wiki/File:Phase_shift.svg

[10] B. Schwab, *Bioelectromagnetics*. University of Twente, 2022.

[11] D. J. GRIFFITHS, *Introduction to electrodynamics*. CAMBRIDGE UNIV PRESS, 2023.

[12] Dec 2016. [Online]. Available: http://www.mathemafrica.org/?p=13232

[13] G. Gaugain, L. Quéguiner, M. Bikson, R. Sauleau, M. Zhadobov, J. Modolo, and D. Nikolayev, "Quasi-static approximation error of electric field analysis for transcranial current stimulation," *Journal of Neural Engineering*, vol. 20, no. 1, p. 016027, 2023.

[14] R. M. Sapolsky, *Behave the biology of humans at our best and worst*. Vintage Books, 2018.

[15] E. Lindberg, "Light-up neuron," Sep 2018. [Online]. Available: https://www.brainfacts.org/for-educators/for-the-classroom/2017/light-up-neuron-092717

[16] F. H. Kasten, K. Duecker, M. C. Maack, A. Meiser, and C. S. Herrmann, "Integrating electric field modeling and neuroimaging to explain inter-individual variability of tacs effects," *Nature Communications*, vol. 10, no. 1, 2019.

[17] T. O. Bergmann and G. Hartwigsen, "Inferring causality from noninvasive brain stimulation in cognitive neuroscience," *Journal of Cognitive Neuroscience*, vol. 33, no. 2, p. 195–225, 2021.

[18] P. Lakatos, J. Gross, and G. Thut, "A new unifying account of the roles of neuronal entrainment," *Current Biology*, vol. 29, no. 18, Sep 2019.

[19] G. B. Saturnino, O. Puonti, J. D. Nielsen, D. Antonenko, K. H. Madsen, and A. Thielscher, "Simnibs 2.1: A comprehensive pipeline for individualized electric field modelling for transcranial brain stimulation," *Pub Med*, 2018.

[20] D. C. Van Essen, S. M. Smith, D. M. Barch, T. E. Behrens, E. Yacoub, and K. Ugurbil, "The wu-minn human connectome project: An overview," *NeuroImage*, vol. 80, p. 62–79, May 2013.

[21] G. B. Saturnino, A. Thielscher, K. H. Madsen, T. R. Knösche, and K. Weise, "A principled approach to conductivity uncertainty analysis in electric field calculations," *NeuroImage*, vol. 188, p. 821–834, Mar 2019.

[22] T. Medani, "Controlling the volume mesh density with headreco · issue 19 · simnibs/simnibs," Feb 2020. [Online]. Available: https://github.com/simnibs/simnibs/issues/19

[23] G. B. Saturnino, K. H. Madsen, H. R. Siebner, and A. Thielscher, "How to target inter-regional phase synchronization with dual-site transcranial alternating current stimulation," *NeuroImage*, vol. 163, p. 68–80, 2017.

[24] R. T. T. nbsp; nbsp; nbsp; nbsp; nbsp; nbsp; nbsp; nbsp; nbsp; 44522 gold badges1010 silver badges2626 bronze badges and L. M. M. nbsp; nbsp; nbsp; nbsp; nbsp; nbsp; nbsp; nbsp; nbsp; 116k77 gold badges7171 silver badges167167 bronze badges, "Calculating a point in 3d using the pythagorean theorem," May 1965. [Online]. Available: https://math.stackexchange.com/questions/3146734/calculating-a-point-in-3d-using-the-pythagorean-theorem

[25] R. Oostenvelt, "2: Electrode positions in the proposed 10-5 system. positions ..." Oct 2022. [Online]. Available: https://www.researchgate.net/figure/Electrode-positions-in-the-proposed-10-5-system-Positions-additional-to-the-10-10_fig6_254876989

VII. APPENDIX

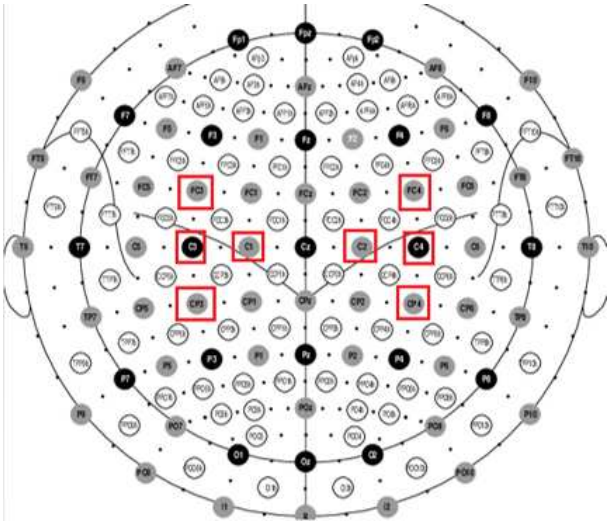

Fig. 22: Montage 1 example, adapted from [25]

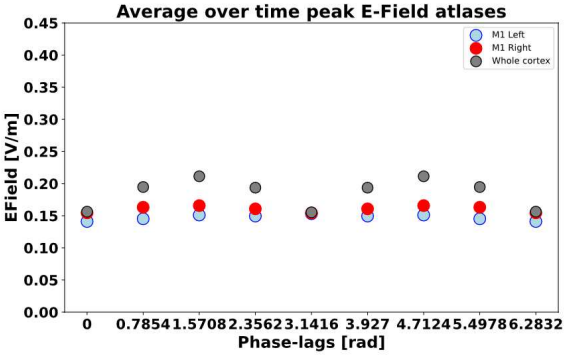

Fig. 23: Example Magnitude Result for One Subject

A. Normalized Dot Product (DotP)

Another measure that was left out due to lack of time was the normalized dot product, which provided a measure for the orthogonality of the field.

$$DotP = \frac{\mathbf{E_n^{in}} \cdot \mathbf{E_n^{in}}}{\left\|\mathbf{E_n^{in}}\right\| \left\|\mathbf{E_n^{in}}\right\|}$$

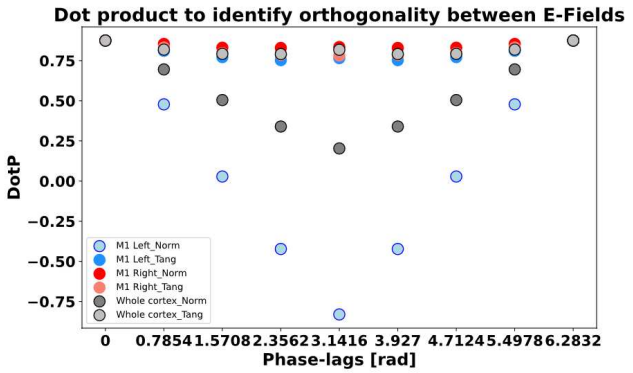

Fig. 24: Example Dot product plot for 1 simulation

However, it should be one for the zero phase lag (Just like in RDM) since dot products with itself is one.

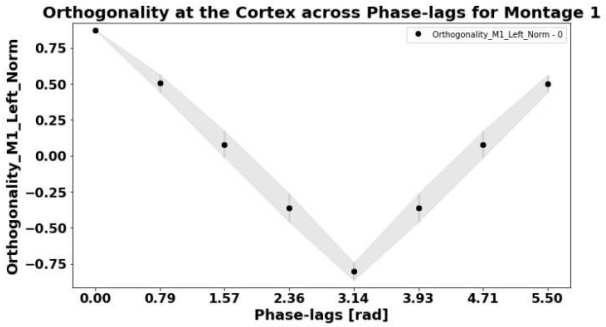

Fig. 25: Left M1 Dot Product

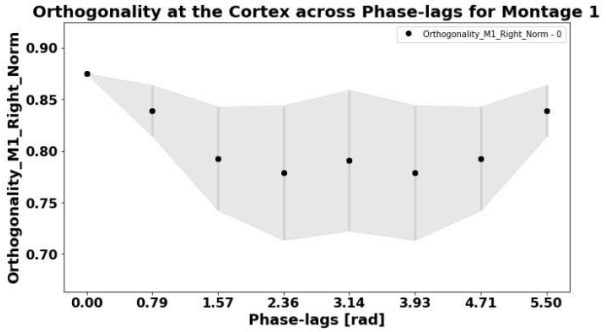

Fig. 26: Right M1 Dot Product

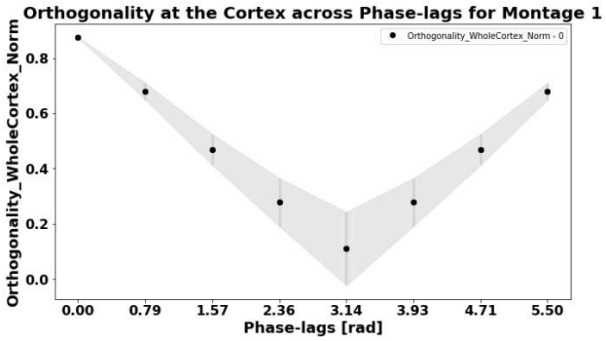

Fig. 27: Whole Cortex M1 Dot Product

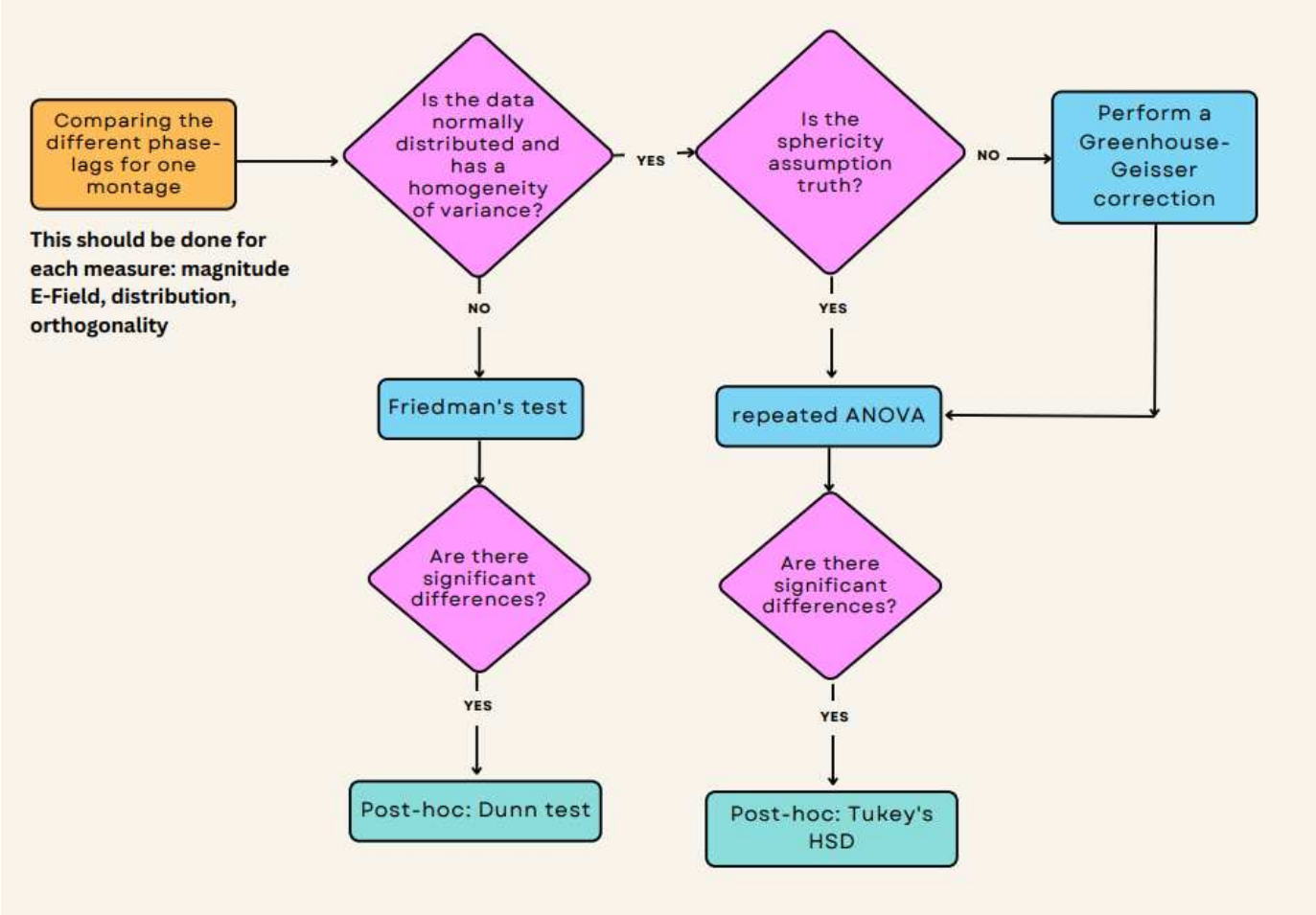

Fig. 28: Statistical test flow chart

Montage	Dep Varia	0	0.7854	1.5708	2.3562	3.1416	3.927	4.7124	5.4978
Multi1	Av_Efield_	nonSig	nonSig	nonSig	nonSig	nonSig	nonSig	nonSig	nonSig
Multi2	Av_Efield_	nonSig	nonSig	0.027	nonSig	nonSig	nonSig	0.027	nonSig
Multi3	Av_Efield_	nonSig	nonSig	nonSig	nonSig	nonSig	nonSig	nonSig	nonSig
Multi1	Av_Efield_	nonSig	nonSig	nonSig	nonSig	nonSig	nonSig	nonSig	nonSig
Multi2	Av_Efield_	nonSig	nonSig	nonSig	nonSig	nonSig	nonSig	nonSig	nonSig
Multi3	Av_Efield_	nonSig	nonSig	nonSig	nonSig	nonSig	nonSig	nonSig	nonSig
Multi1	Av_Efield_	nonSig	nonSig	nonSig	nonSig	nonSig	nonSig	nonSig	nonSig
Multi2	Av_Efield_	nonSig	nonSig	nonSig	nonSig	nonSig	nonSig	nonSig	nonSig
Multi3	Av_Efield_	nonSig	nonSig	nonSig	nonSig	nonSig	nonSig	nonSig	nonSig

Fig. 29: Statistical test Results for Average field Strength per Montage. nonSig is shown when the pvalue is above 0.05

Montage	Dep Variable	0	0.7854	1.5708	2.3562	3.1416	3.927	4.7124	5.4978
Multi1	RDM_M1_Left_Norm	nonSig	nonSig	0	0	0	0	0	nonSig
Multi2	RDM_M1_Left_Norm	nonSig	nonSig	0	0	0	0	0	nonSig
Multi3	RDM_M1_Left_Norm	nonSig	nonSig	0	0	0	0	0	nonSig
Multi1	RDM_M1_Left_Tang	nonSig	nonSig	0	0	0	0	0	nonSig
Multi2	RDM_M1_Left_Tang	nonSig	nonSig	0	0	0	0	0	nonSig
Multi3	RDM_M1_Left_Tang	nonSig	nonSig	0	0	0	0	0	nonSig
Multi1	RDM_M1_Right_Norm	nonSig	nonSig	0	0	0	0	0	nonSig
Multi2	RDM_M1_Right_Norm	nonSig	nonSig	0	0	0	0	0	nonSig
Multi3	RDM_M1_Right_Norm	nonSig	nonSig	0	0	0	0	0	nonSig
Multi1	RDM_M1_Right_Tang	nonSig	nonSig	0	0	0	0	0	nonSig
Multi2	RDM_M1_Right_Tang	nonSig	nonSig	0	0	0	0	0	nonSig
Multi3	RDM_M1_Right_Tang	nonSig	nonSig	0	0	0	0	0	nonSig
Multi1	RDM_WholeCortex_Norm	nonSig	nonSig	0	0	0	0	0	nonSig
Multi2	RDM_WholeCortex_Norm	nonSig	nonSig	0	0	0.003	0	0	nonSig
Multi3	RDM_WholeCortex_Norm	nonSig	nonSig	0	0	0	0	0	nonSig
Multi1	RDM_WholeCortex_Tang	nonSig	nonSig	0	0	0.049	0	0	nonSig
Multi2	RDM_WholeCortex_Tang	nonSig	nonSig	0	0	nonSig	0	0	nonSig
Multi3	RDM_WholeCortex_Tang	nonSig	nonSig	0	0	0.034	0	0	nonSig

Fig. 30: Statistical test Results for RDM per Montage. nonSig is shown when the pvalue is above 0.05